ELECTROMAGNETIC INTERACTIONS WITH ROUGH METAL SURFACES

F. J. Garcia-Vidal and J. B. Pendry

The Blackett Laboratory, Imperial College, London SW7 2BZ, U.K.

Abstract

When surfaces are structured on the scale of the wavelength, we can expect incident light to be strongly modified by the surface. This is especially the case when the surface is metallic. We have developed a formalism for computing these modifications, closely analogous to electron scattering theory, which we briefly review and present some results for optical properties of, and electron energy loss in, colloids. Our main theme is another effect associate with rough or structured metallic surfaces: Surface Enhanced Raman Scattering, or SERS. We model the rough surface by a periodic array of spheres and obtain the correct magnitude for the enhancement and for the frequency shifts observed.

Acronyms

SERS   Surface Enhanced Raman Scattering

1. Introduction

Metals are distinguished in their electromagnetic properties by having in the visible and ultra violet part of the spectrum a *negative* dielectric function which typically takes the form,

$$\varepsilon(\omega) = 1 - \frac{\omega_p^2}{\omega^2}$$

(1)

This is the classical plasma resonant form with ε vanishing at $\omega = \omega_p$, the frequency of the bulk plasma resonance. In this approximation the bulk resonance is completely decoupled from external electromagnetic fields and can only be excited by charged particles which penetrate inside the metal.

This form of ε also gives the metallic surface a series of very interesting resonances. For example a flat surface supports a surface plasmon at,

$$\omega_{sp} = \omega_p / \sqrt{2} \tag{2}$$

and a spherical surface has a whole series of resonances whose frequencies depend on the angular momentum, ℓ,

$$\omega_{sphere} = \sqrt{\frac{\ell}{2\ell+1}} \omega_p \tag{3}$$

In general, the more complex the surface, the more interesting are the associated plasma modes. In particular, surfaces that are *rough* have extremely complex modes which have many consequences both for their interaction with charged particles and with incident electromagnetic waves. The former we have investigated in some detail. In this paper we shall concentrate on the latter.

One commonly observed consequence of surface roughness is seen in the blackness of *collections* of finely divided metal particles such as colloids. We stress collections because isolated colloidal particles typically show absorption only in the ultra violet, at the surface plasmon frequency in fact. It is the mutual interaction of the particles that produces the effect and these interactions must be strong enough and complex enough to produce broad band absorption at very much lower frequencies than the original surface plasmon resonance.

Perhaps the most celebrated effect is Surface Enhanced Raman Scattering (SERS) first observed by Fleischmann et al [1]. In these experiments laser light is scattered from molecules adsorbed on a surface. Some of the photons will lose energy to the vibrational modes of the molecules and be scattered at a slightly lower frequency. The gas phase cross-section for this process would suggest that the Raman signal would be rather weak, but for certain instances, especially for rough silver surfaces, the signal is enhanced, perhaps by as much as a factor of a million. On these surfaces interaction of the incident and reflected wave fields with the resonant modes of the rough surface produces very intense local fields which give rise to the enhanced cross section. In fact, since the matrix element for the Raman process is proportional to both incident and reflected wave fields, the intensity of the final signal scales as $|E_0|^4$, where E_0 is the incident wavefield amplitude before it hits the surface.

It has long been recognised that the enhancement is a collective effect because enhancement at a single metal sphere or spheroid can easily be calculated and does not even come close to the values observed. More sophisticated treatments [2] seek to represent the collective nature of the phenomenon

by taking an ordered array of spheres as a model for the rough surface. Calculating the electric fields even in this simple model is by no means trivial and previous attempts have made approximations such as calculating the sphere-sphere interactions in the dipole approximation. This is only accurate in the limit that the spheres are far apart and in general many multipoles are needed in the expansion. This was recognised by Xu and Dignam [3] who included the multipole terms but were limited to a linear array of spheres. Although they did calculate very large enhancements there is still some question of whether the 2D nature of the problem is vital. One may suspect that it is, because interaction between a pair of spheres, even when carried to very high order in the multipole expansion, is not sufficient to account for the SERS enhancement.

In the next section we present a different way forward, adopting the model of an ordered array of spheres, see Fig. 1.
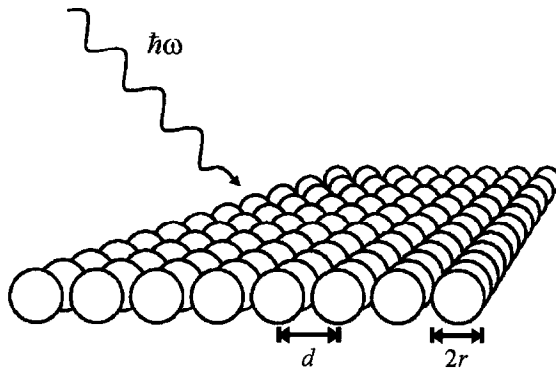
Fig. 1. A rough metal surface is modelled by a simple square array of metal spheres, diameter $2r$, lattice spacing d. Typically $d = 20$nm, $2r = 10$nm.

2. Theory of Light in Complex Structures

Recently there has been a great deal of interest in so called photonic materials which are structured on the scale of the wavelength of light [4, 5, 6, 7]. The original thrust of this work was to find a periodic dielectric structure which shows an absolute band gap: a photonic insulator. It has been necessary to develop new techniques for solving Maxwell's equations in these structured materials. The methodology we developed [7, 8] is particularly well suited to metals because the calculation proceeds at constant frequency. In this section we give a brief guide to the theory.

In order to compute the fields inside a structure we approximate the continuous fields by their values at a series of discrete points located on a simple cubic lattice, unit cell of side a. We wish to

find a valid approximation to Maxwell's equations for these discrete fields, We start from Maxwell's equations:

$$\nabla \times \mathbf{E} = -\partial \mathbf{B} / \partial t, \tag{4}$$

$$\nabla \times \mathbf{H} = +\partial \mathbf{D} / \partial t, \tag{5}$$

and assume that,

$$\mathbf{B} = \mu_0 \mathbf{H}, \tag{6}$$

hence,

$$\nabla \times \nabla \times \mathbf{E} = -\mu_0 \partial^2 \mathbf{D} / \partial t^2 = \varepsilon(\mathbf{r}) c_0^{-2} \partial^2 \mathbf{E} / \partial t^2$$
$$= -\nabla^2 \mathbf{E} + \nabla(\nabla \cdot \mathbf{E}) \tag{7}$$

Transforming to $\mathbf{k}, \omega$ space:

$$(\mathbf{k} \cdot \mathbf{k}) \mathbf{E}(\mathbf{k}) - \mathbf{k}\big(\mathbf{k} \cdot \mathbf{E}(\mathbf{k})\big) = \omega^2 c_0^{-2} \sum_{\mathbf{k}'} \varepsilon(\mathbf{k}, \mathbf{k}') \mathbf{E}(\mathbf{k}') \tag{8}$$

Note the outer product in the second term on the left hand side: its function is to ensure that the longitudinal modes have zero frequency. Any mode that is polarised perpendicular to $\mathbf{k}$ obeys the normal Laplacian equation. The strategy we employ is to discretise this equation approximating $\mathbf{k} \cdot \mathbf{k}$ and $\mathbf{k} \times \mathbf{k}$ by sines and cosines. By retaining the form of an outer product we ensure that one of the three modes is always of zero frequency and therefore plays no part in transport. On transforming back into real space, expressions like $\exp(ik_x a)$ give rise to terms coupling to some neighbour. The lattice structure is defined by the choice of approximation, as is the occurrence of first, second, ... nearest neighbours. Approximate (8) by,

$$a^{-2} \sum_j \left\{ \begin{array}{l} \left[\left| \exp(ik_x a) - 1 \right|^2 + \left| \exp(ik_y a) - 1 \right|^2 + \left| \exp(ik_z a) - 1 \right|^2 \right] \delta_{ij} \\ -\left[(\exp(+ik_i a) - 1)(\exp(-ik_j a) - 1) \right] \end{array} \right\} E_j$$

$$= \omega^2 c_0^{-2} \sum_{\mathbf{k}'} \varepsilon(\mathbf{k}, \mathbf{k}') E_i(\mathbf{k}') \tag{9}$$

On transforming back into real space we get 3×3 blocks of elements relating to sites on a simple cubic lattice, extending to next nearest neighbour interactions. However it is advantageous to stay with a set of coupled first order equations for the $\mathbf{E}$ and $\mathbf{H}$ fields when it comes to a numerical implementation of the formulae. Transforming (4) and (5) into k, ω space we have,

$$\mathbf{k} \times \mathbf{E} = +\omega\mathbf{B}, \tag{10a}$$

$$\mathbf{k} \times \mathbf{H} = -\omega\mathbf{D}. \tag{10b}$$

In (10a,b) we approximate,

$$\mathbf{k}_x \approx (+ia)^{-1}[\exp(+ik_x a) - 1], \text{ etcetera}, \tag{11a}$$

$$\mathbf{k}_x \approx (-ia)^{-1}[\exp(-ik_x a) - 1], \text{ etcetera}, \tag{11b}$$

Transforming back into real space gives a set of equations from which the z- components of the vectors can be eliminated, and the substitution,

$$\mathbf{H'} = \frac{+i}{a\omega\varepsilon_0}\mathbf{H} \tag{12}$$

made to give,

$$
\begin{aligned}
\mathbf{E}_x(\mathbf{r}+\mathbf{c}) = {}& \mathbf{E}_x(\mathbf{r}) + \frac{c^2\omega^2}{c_0^2}\mu(\mathbf{r})\mathbf{H'}_y(\mathbf{r}) \\
& + \frac{c^2}{a\varepsilon(\mathbf{r})}\begin{bmatrix} +a^{-1}\{\mathbf{H'}_y(\mathbf{r}-\mathbf{a})-\mathbf{H'}_y(\mathbf{r})\} \\ -b^{-1}\{\mathbf{H'}_x(\mathbf{r}-\mathbf{b})-\mathbf{H'}_x(\mathbf{r})\} \end{bmatrix} \\
& \frac{-c^2}{a\varepsilon(\mathbf{r}+\mathbf{a})}\begin{bmatrix} +a^{-1}\{\mathbf{H'}_y(\mathbf{r})-\mathbf{H'}_y(\mathbf{r}+\mathbf{a})\} \\ -b^{-1}\{\mathbf{H'}_x(\mathbf{r}+\mathbf{a}-\mathbf{b})-\mathbf{H'}_x(\mathbf{r}+\mathbf{a})\} \end{bmatrix}
\end{aligned}
\tag{13}
$$

$$
\begin{aligned}
\mathbf{E}_y(\mathbf{r}+\mathbf{c}) = {}& \mathbf{E}_y(\mathbf{r}) - \frac{c^2\omega^2}{c_0^2}\mu(\mathbf{r})\mathbf{H'}_x \\
& \frac{c^2}{b\varepsilon(\mathbf{r})}\begin{bmatrix} +a^{-1}\{\mathbf{H'}_y(\mathbf{r}-\mathbf{a})-\mathbf{H'}_y(\mathbf{r})\} \\ -b^{-1}\{\mathbf{H'}_x(\mathbf{r}-\mathbf{b})-\mathbf{H'}_x(\mathbf{r})\} \end{bmatrix} \\
& \frac{-c^2}{b\varepsilon(\mathbf{r}+\mathbf{b})}\begin{bmatrix} +a^{-1}\{\mathbf{H'}_y(\mathbf{r}-\mathbf{a}+\mathbf{b})-\mathbf{H'}_y(\mathbf{r}+\mathbf{b})\} \\ -b^{-1}\{\mathbf{H'}_x(\mathbf{r})-\mathbf{H'}_x(\mathbf{r}+\mathbf{b})\} \end{bmatrix}
\end{aligned}
\tag{14}
$$

$$
\begin{aligned}
\mathbf{H'}_x(\mathbf{r}+\mathbf{c}) = {}& \mathbf{H'}_x(\mathbf{r}) + \varepsilon(\mathbf{r}+\mathbf{c})\mathbf{E}_y(\mathbf{r}+\mathbf{c}) \\
& \frac{-c_0^2}{a\omega^2\mu(\mathbf{r}-\mathbf{a}+\mathbf{c})}\begin{bmatrix} +a^{-1}\{\mathbf{E}_y(\mathbf{r}+\mathbf{c})-\mathbf{E}_y(\mathbf{r}-\mathbf{a}+\mathbf{c})\} \\ -b^{-1}\{\mathbf{E}_x(\mathbf{r}-\mathbf{a}+\mathbf{b}+\mathbf{c})-\mathbf{E}_x(\mathbf{r}-\mathbf{a}+\mathbf{c})\} \end{bmatrix} \\
& \frac{+c_0^2}{a\omega^2\mu(\mathbf{r}+\mathbf{c})}\begin{bmatrix} +a^{-1}\{\mathbf{E}_y(\mathbf{r}+\mathbf{a}+\mathbf{c})-\mathbf{E}_y(\mathbf{r}+\mathbf{c})\} \\ -b^{-1}\{\mathbf{E}_x(\mathbf{r}+\mathbf{b}+\mathbf{c})-\mathbf{E}_x(\mathbf{r}+\mathbf{c})\} \end{bmatrix}
\end{aligned}
\tag{15}
$$

$$\mathbf{H'}_y(\mathbf{r}+\mathbf{c})] = \mathbf{H'}_y(\mathbf{r}) - \varepsilon(\mathbf{r}+\mathbf{c})\mathbf{E}_x(\mathbf{r}+\mathbf{c})$$

$$\frac{-c_0^2}{b\omega^2\mu(\mathbf{r}-\mathbf{b}+\mathbf{c})}\left[\begin{array}{l}+a^{-1}\{\mathbf{E}_y(\mathbf{r}+\mathbf{a}-\mathbf{b}+\mathbf{c})-\mathbf{E}_y(\mathbf{r}-\mathbf{b}+\mathbf{c})\}\\-b^{-1}\{\mathbf{E}_x(\mathbf{r}+\mathbf{c})-\mathbf{E}_x(\mathbf{r}-\mathbf{b}+\mathbf{c})\}\end{array}\right]$$

$$\frac{+c_0^2}{b\omega^2\mu(\mathbf{r}+\mathbf{c})}\left[\begin{array}{l}+a^{-1}\{\mathbf{E}_y(\mathbf{r}+\mathbf{a}+\mathbf{c})-\mathbf{E}_y(\mathbf{r}+\mathbf{c})\}\\-b^{-1}\{\mathbf{E}_x(\mathbf{r}+\mathbf{b}+\mathbf{c})-\mathbf{E}_x(\mathbf{r}+\mathbf{c})\}\end{array}\right] \tag{16}$$

The simple cubic mesh on which we define the fields is defined by vectors $\mathbf{a}$, $\mathbf{b}$, $\mathbf{c}$, of length a, b, c, which point in the x, y, z, directions respectively. The first two equations express the **E**- field on the next plane of cells in terms of the **E**- and **H**- fields on the previous plane. The second pair of equations express the **H**- fields on the next plane of cells in terms of the **E**- on the same plane, and the **H**- fields on the previous plane. Thus given the x, y, components of the **E**- and **H**- fields on one side of a dielectric structure, we can integrate through the structure to find the x, y, components of the **E**- and **H**- fields on the other side. Incidentally, if we wish, we can also use subsidiary equations to calculate the z- components too. The matrix relating fields on one side of a structure to those on the other is by definition the *transfer matrix*. Where the structure is the unit cell of a periodic array, the eigenvalues of the transfer matrix give the band structure of the system. It will be noted that the transfer matrix works at constant frequency and is therefore an ideal tool for handling metallic structures where the dielectric function depends strongly on frequency.

3. Some Calculations Using the New Theory

It is instructive to calculate the photonic band structure for a simple cubic array of metal spheres which might represent a dense metallic colloid or a rough metallic surface. In Fig. 2 we show a calculation for an array of aluminium spheres in which the metallic dielectric function takes the plasma resonant form shown in (1) with a plasma frequency of 15eV. We deliberated neglect resistive losses in order to display the underlying resonant structure of the states.

The band structure gives insight into the SERS experiments and we shall spend a few moments discussing it. First note that for isolated spheres all the modes lie in the range $15/\sqrt{3}$eV to $15/\sqrt{2}$eV (8.7eV to 10.6eV). and it is evident that even for this relatively dilute lattice, with a volume filling fraction of only 12%, there is a very substantial shift of frequencies from the isolated sphere values. Furthermore, since there are only three independent dipole modes associated with a sphere and we see here many more than three modes displaced to low frequencies, the shift must be due to strong multipole interactions between the spheres. Second, we can see that nearly all the modes correspond
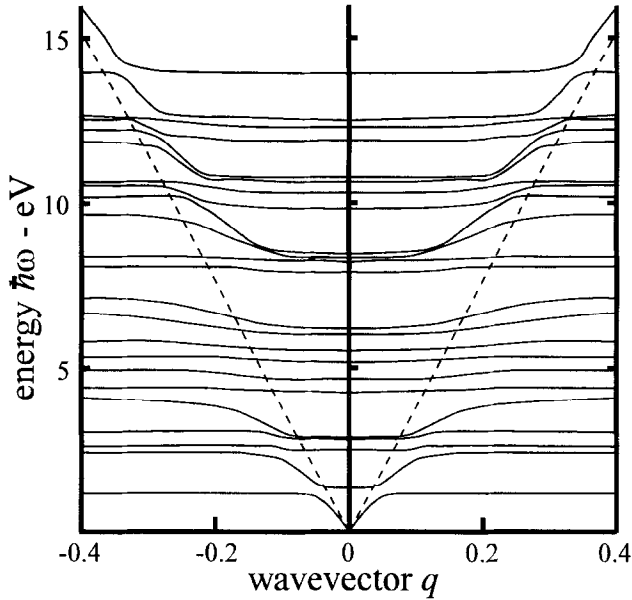
Fig. 2. The electromagnetic band structure of a simple cubic array of metal spheres calculated for loss-free aluminium. The lattice spacing is 5.29nm and the sphere radius 1.6nm. Note the characteristic structure which consists of a large number of extremely flat bands: these are surface plasma modes of the metal spheres, found in the range 8.7eV to 10.6eV for isolated spheres, but in this instance spread to a lower range of energies by interaction between spheres. The free space dispersion relation is shown as a dashed line, and clearly interacts strongly with the surface modes.

to very 'flat' bands with low group velocity. This implies that the states are highly localised in space. Obviously they are not localised on the spheres because their frequencies do not correspond to those of an isolated sphere, rather these are modes trapped between several spheres emphasising the collective nature of the electromagnetic structure. Third, we can make an alternative interpretation of the flat band structure by regarding the individual bands as resonant states and interpreting the band width as the lifetime of these resonances. With this interpretation we see that some of the states have a Q-factor of around 100 or more implying that the electric field intensities are enhanced by a factor of 100 when trapped in a resonance. The Raman signal scales as $|\mathbf{E}|^4$ thus implying enhancements of 10^4 or more, at least for loss free metals. The highly resonant features also explain why Raman enhancement is sensitive to the metal conductivity: high conductivity materials will preserve the resonances in a relatively undamped state. In resistive samples resonances will be heavily damped, their Q-factor and the Raman enhancement being correspondingly reduced.

Using our theory it is relatively straightforward to calculate the reflection coefficient of a surface. We might expect that a surface of the metal sphere lattice would be highly absorbing to light because

of the many resonant bands able to trap the light. Certainly these bands couple strongly to incident radiation as can be seen from Fig. 2 where they clearly hybridise with the free space transverse modes. We show below in Fig.3 our calculations of reflection from and transmission through a sample of our aluminium sphere lattice. This time we include the resistive losses.
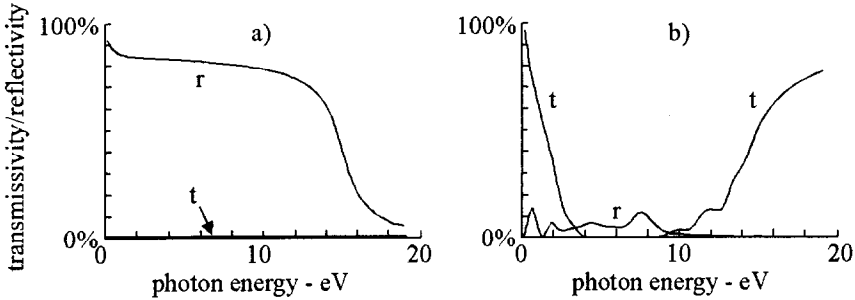
Fig. 3. The contrasting reflectivity and transmissivity of, a) solid metal, and b) that of a colloidal array of 1.6nm radius metal spheres filling 12% of the sample volume. The thickness of material considered is 338.5nm in both cases.

Note that solid metal absorbs little light in the visible frequency range because there are no modes in which to deposit the energy. In contrast the colloidal lattice is highly absorbing due to the new modes which couple strongly to incident light. This feature has led to close coupled colloids being employed in solar heating systems: their excellent absorbing properties in the visible region soak up the sunshine, but the absence of modes in the infra red makes them poor emitters. Thus a structure made from a metal colloid will retain the heat.

4. Simulating SERS Experiments

We shall adopt a 2D ordered array of metallic spheres as our model of a rough surface as shown in Fig. 1. This model has been successfully employed to describe optical properties of colloids, and their interaction with high energy electron beams [9]. We modelled the dielectric function of silver by [10],

$$\varepsilon(\omega) = 5.7 - \omega_p^2 \Big/ \omega^2 + i\gamma, \; \omega_p = 9.0eV, \gamma = 0.4 \tag{17}$$

Assuming that light is incident normal to the surface and that the Raman signal is also measured at or near normal emission, we calculated the reflection coefficient for light normally incident on our 2D array. Thus we can find the total wavefield, incident plus reflected, outside the surface. Next the wavefield was integrated back into the array and a detailed picture of the wave field around the spheres was obtained. It was assumed that the Raman active molecules were adsorbed on the surface

of the spheres and therefore to calculate the Raman enhancement we averaged $|\mathbf{E}_s|^4$ over the entire surface of a sphere. If the incident field is $\mathbf{E}_0$ then the Raman enhancement is simply,

$$< |\mathbf{E}_s|^4 > / |\mathbf{E}_0|^4 \tag{18}$$

We show below in Fig. 4 the results of this calculation.
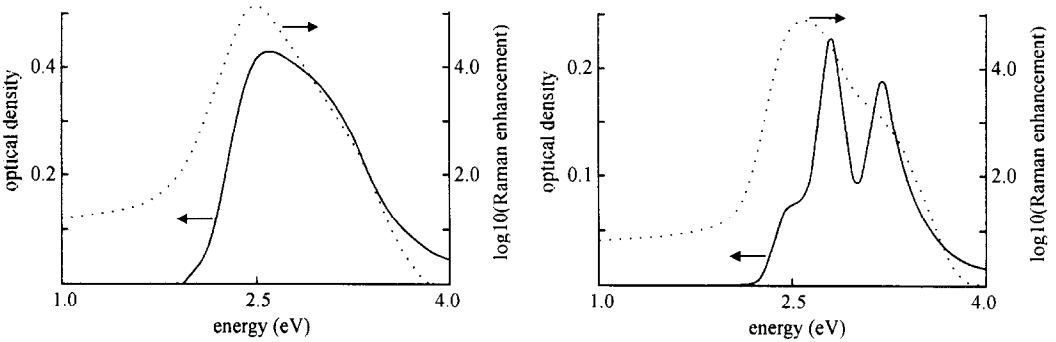
Fig. 4. Calculated surface enhanced Raman signal excitation spectrum for a layer of silver spheres as shown in Fig. 1. Left: $d = 12$nm, $r = 5$nm ($r/d = 0.42$), right: $d = 20$nm, $r = 5$nm ($r/d = 0.25$). The cross sections of spheres cover 50% and 19.6% of the area respectively. Solid line: extinction spectrum, dotted line: Raman enhancement.
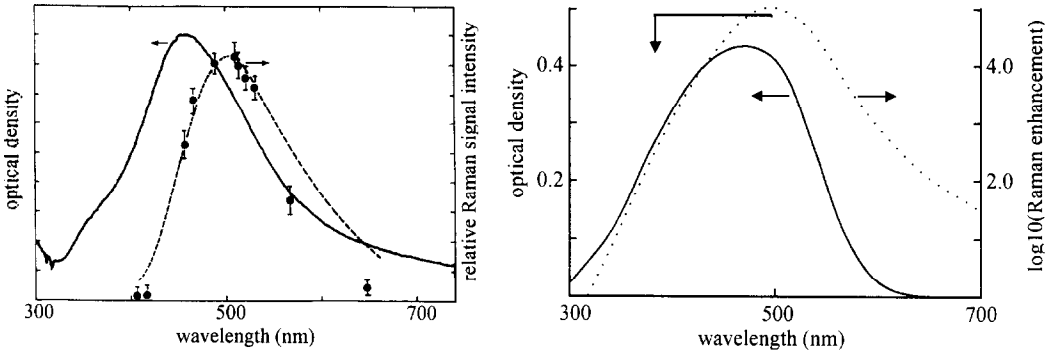
Fig. 5. Left: experimental surface enhanced Raman signal excitation spectrum for nitrobenzoate on a silver-island film (dashed line) together with the extinction spectrum (solid line), taken from ref [10]. Right: our calculated enhancement for $r/d = 0.4$, showing the shift of the enhancement peak from the dipole resonance of an isolated silver sphere (vertical arrow). The peak enhancement of experiment, relative to results in solution, is roughly 10^5, in good general agreement with our calculations.

Note that the enhancement for this relatively dilute lattice of spheres is around 10^5 in rough agreement with experiments. In fact some closely related experiments have been made by Weitz et al

[11]. Their results are shown in Fig. 5 compared to our calculations replotted against wavelength rather than frequency,

Note that our theory predicts not only the correct positions of both absorption and enhancement peaks but, most important of all, the correct degree of enhancement. We conclude that, in common with the optical and electron energy loss properties of colloids, SERS experiments can be modelled reliably by an ordered surface of metal spheres with a filling fraction appropriate to the surface roughness.

In the light of our ability to make calculations for ordered surfaces, it will be interesting to explore further the nature of SERS from ordered arrays of metallic quantum dots.

5. Acknowledgements

6. References

1. M. Fleischmann, P.J. Hendra, and A.J. Mcquillan, Chem. Phys. Lett., **26**, 163 (1974).
2. L.C. Chu and S.Y. Wang, Phys. Rev. **B31**, 693 (1985).
3. M. Xu and M.J. Dignam, J.Chem. Phys., **100**, 197 (1994).
4. E. Yablonovitch, T.J. Gmitter, and K.M. Leung, Phys. Rev. Lett., **67**, 2295 (1991).
5. K.M. Ho, C.T. Chan, and C.M. Soukoulis, Phys. Rev. Lett., **65**, 3152 (1991).
6. J.B. Pendry and A. MacKinnon, Phys. Rev. Lett. **69** 2772 (1992).
7. J.B. Pendry, J. Mod. Optics **41** 209 (1994).
8. P. M. Bell, J.B. Pendry, L. Martín-Moreno, and A.J. Ward, Comp. Phys. Comm., **85** 306 (1995).
9. J.B. Pendry and L. Martín-Moreno, Phys. Rev., **B50**, 5062 (1994).
10. P.B. Johnson and R.W. Christy, Phys. Rev., **B6**, 4370 (1972).
11. D.A. Weitz, S. Garoff, and T.J. Gamila, Opt. Lett. 7, 89 (1982).